A Transient Hydrodynamic Model of Screen Channel Liquid Acquisition Devices for In-space Cryogenic Propellant Management

C. F. Camarotti [1], J. W. Hartwig [2], H. Wang [1], J. N. Chung [1]
[1]*Department of Mechanical and Aerospace Engineering, University of Florida, Gainesville, FL 32611, USA*
[2]*NASA Glenn Research Center, Cleveland, Ohio 44135, USA*

ABSTRACT

Screen channel liquid acquisition devices (LADs) will play a crucial role in future deep space travel. It is essential that vapor-free delivery of propellants during tank-to-tank transfer is ensured to maximize yield from storage tanks and prevent potential combustion instabilities. The screen channel LAD utilizes a fine screen wire mesh that can separate phases in a low Bond number (i.e. microgravity) environment using surface tension forces. This study presents the development and verification of a new model for transient screen compliance, one of the influential factors for screen channel LAD design. Screen compliance is crucial during LAD channel outflow transients because the slight deflection of the screen can provide needed mass to satisfy rapid outflow demands and reduce the pressure difference across the screen. The model is successfully verified against CFD simulations. In addition, the characteristic speed for the governing screen compliance equations is derived which allows for numerical stability criteria to be established. As shown in this study, the transient maximum pressure difference across the screen can greatly exceed the steady state maximum pressure difference across the screen in many cases.

NOMENCLATURE

A_{CH}	Cross sectional area of channel	t_{open}	Valve opening time
A_{SC}	Open area of the screen	T_{SC}	Effective screen deflection thickness
$\bar{\bar{A}}$	Jacobian matrix	T_{SC_0}	Initial effective screen deflection thickness at rest
a_{SC}	Acceleration of fluid	T_{ij}	Stress tensor in momentum equation
C_{lam}	Armour and Cannon FTS constant	$\vec{U}$	Conserved variable vector
C_{turb}	Armour and Cannon FTS constant	u	Velocity of liquid in channel
D_P	Effective pore diameter of screen	u_{avg}	Average velocity
d_s	Shute wire diameter of screen	$u_{characteristic}$	Characteristic speed
dt	Time step	u_{demand}	Steady state demand velocity
dx	Spatial grid size	V_{SC}	Volume of liquid extracted underneath screen
$Error_M$	Error for given mesh size	v_{inj}	Injection velocity into channel across screen
e	Screen channel roughness	w_{SC}	Width of channel screen
$\vec{F}$	Flux vector	x	Dimension along the length of the channel
f	Function solved in 2D steady channel outflow model	z	Height relative to the acceleration vector
g	Gravitational acceleration	α	Armour and Cannon fitting coefficient
H	Cross sectional height of the channel	β	Armour and Cannon fitting coefficient
K_{SC}	Screen compliance constant	ΔH	Head difference
L	Length of the channel	ΔP_{BP}	Bubble point pressure
M	Mesh size	$\Delta P_{dynamic}$	Dynamic pressure drop along channel
$\dot{m}$	Demand mass flow rate	$\Delta P_{frictional}$	Frictional pressure drop along channel
N	Number of grid points	ΔP_{FTS}	Flow through screen pressure drop
p	Rate of convergence	$\Delta P_{hydrostatic}$	Hydrostatic pressure drop along channel
$P_{channel}$	Pressure inside the LAD channel	ΔP_{SC}	Pressure difference between liquid and vapor side of screen
P_{gas}	Gas screen side pressure	$\Delta P_{SC}'$	Pressure difference between vapor and liquid side of screen (i.e. $\Delta P_{SC}' = -\Delta P_{SC}$)
P_{liq}	Liquid screen side pressure	λ_n	Eigenvalues for viscous pressure drop model
P_0	Pressure outside the LAD channel	$\lambda^{\pm}$	Eigen values of the Jacobian matrix
s_{SC}	Wetted perimeter of the channel cross sectional area	μ	Dynamic viscosity of liquid inside channel
S	Wave speed of Heaviside step function	ρ	Density
$\vec{S}$	Source term vector	ν	Kinematic viscosity of liquid inside channel
t	Time		
Subscripts			
$exposed$	Exposed portion of channel	SS	Steady state
max	Maximum	$total$	Total length of channel
$submerged$	Submerged portion of channel		

I. INTRODUCTION

A. Background

Screen channel liquid acquisition devices (LADs) will play a crucial role in future deep space travel. It is essential that vapor-free delivery of propellants during tank-to-tank transfer is ensured to maximize yield from storage tanks and prevent potential combustion instabilities. The screen channel LAD utilizes a fine screen wire mesh that can separate phases in a low Bond number (i.e. microgravity) environment using surface tension forces.

B. Problem statement

Suppose that during a transient liquid acquisition device (LAD) outflow operation (i.e. engine start up, thruster pulsing, etc.) only a portion of the LAD channel is wetted on both sides of the screen. Prior to demand, there is liquid on the channel side of the screen and vapor on the tank side of the screen near the outlet port of the LAD channel as shown in Fig. 1 [1]. Upon initiating the transient operation, the outlet port demands some volumetric flow rate in a rapid fashion. Therefore, the liquid inside the channel must be accelerated from a zero velocity to a steady state velocity to accommodate this demand. The portion of liquid that is near the outlet will be rapidly outflowed from the channel due to the transient demand flow rate. Liquid further away from the outlet will take longer to leave the channel due to inertial differences, thus creating a pressure gradient along the channel. To alleviate the pressure gradient along the channel, the LAD screen will deflect (i.e. comply) by an effective deflection thickness, T_{SC}, to provide the mass required by the transient demand flow.

The analysis in this study will neglect the curvature effects of the channel along the tank walls and simply consider the screen compliance scenario shown schematically in Fig. 2. This figure shows how the transient 1D screen compliance solver from this study is used for the exposed end of the channel and a 2D outflow solver is used for the submerged portion of the channel. The analysis in this study will solve for the velocity, u, effective deflection thickness, T_{SC}, pressure difference across the screen, ΔP_{SC}, and the injection velocity, v_{inj}, along the entire length of the channel as a function of time during a transient outflow operation.

The differential control volume of a channel fluid element used in this analysis is shown in Fig. 3 [1]. The control volume is a differential element along the exposed portion of the LAD channel and has a non-rigid boundary representing the LAD screen. Surface tension within the pores of the screen provides the necessary force needed to deflect the screen by some effective thickness, T_{SC}. The inward deflection of the screen can provide the small amount of mass required during transient outflow via volumetric displacement, thus satisfying continuity and helping to prevent vapor ingestion into the channel. If the screen was rigid and unable to provide that small mass, the pressure differential across the screen would spike during a transient operation and exceed the bubble point pressure of the screen where the bubble point is defined as the pressure difference across the screen that allows for vapor bubbles to be ingested into the LAD channel (i.e. the screen channel LAD is broken down).

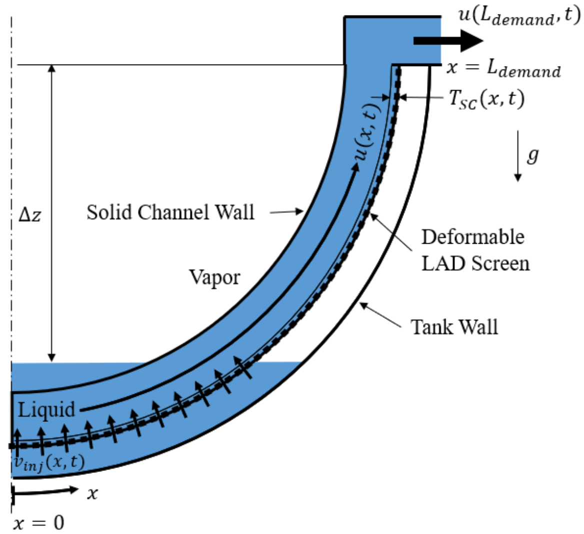

Fig. 1. Scenario where screen compliance is crucial for transient LAD outflow operation. Figure is adapted from Jaekle [1] with additional features added. Note that LAD channel presented in figure has a rectangular cross-sectional area.

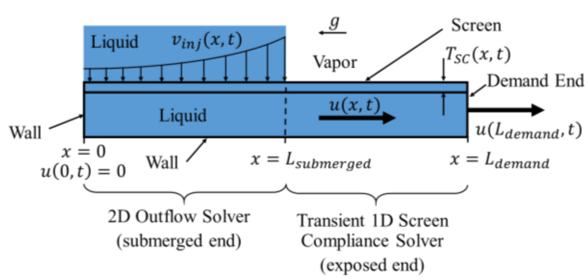

Fig. 2. Simple schematic of a partially submerged screen channel LAD undergoing transient screen compliance. Note that most of the analysis in this study applies the 2D outflow solver to the submerged end of the channel, but the ANSYS Fluent comparison uses a simplified 1D outflow solver for comparison to the transient screen compliance solver.

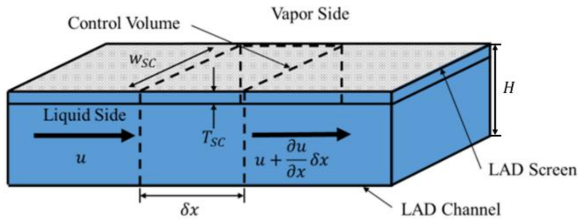

Fig. 3. Control volume used for screen compliance analysis. Note that this figure is adapted from Jaekle 1997 [1].

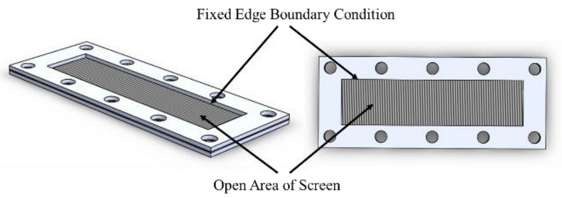

Fig. 4. Example of open area of the screen with fixed edge boundary conditions.

The deflection of the screen due to the differential pressure across it is known as screen compliance. This "deflection" can come from either the screen itself bending, liquid being withdrawn from the pores of the screen, or a combination of both mechanisms. In this analysis, the screen will be considered to deflect by an effective thickness, T_{SC}, which is essentially an averaged deflection across the open area of the screen. The open area of the screen is the portion of the screen that undergoes deflection with all boundary conditions fixed. An example of this definition is illustrated in Fig. 4. Here, a screen sample is fixed between two shims creating a screen assembly with an open area. These types of screen assemblies were used in previous studies that determined values for the screen compliance constant, K_{SC}. There are no other support features across the open area of the screen except for the fixed edge boundary conditions. Also, the two shims that the screen is fixed are of a flat design and do not create any controlled pretension in the screen.

The experiments conducted by Camarotti et al. 2019 [2] identified multiple regions of transient screen compliance. An example of the different regions is provided in Fig. 5 that was initially given in the Camarotti et al. 2019 paper. The initial region represents the liquid vapor interface being above the pores of the screen (i.e. there is a thin layer of liquid on top of the screen). Once the interface enters the pores of the screen, surface tension forces begin to pull the screen taut and retract slack. Once this slack is retracted, the screen enters a linear region of pure deflection up until bubble point is reached.

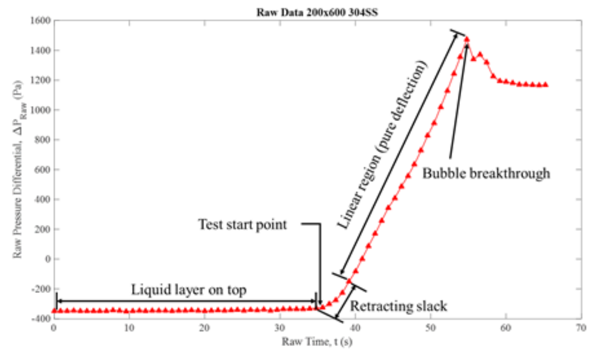

Fig. 5. Different regions of screen compliance identified in Camarotti et al. 2019 [2].

C. Previous studies

Experimental studies of screen compliance available to the public are very limited. Paynter 1973 [3] conducted a series of "Screen Structural Characteristics Tests" where four different circular screen samples were tested using static loading, cyclic loading, and rupture testing techniques while measuring deflection at different radial positions across the screen. The screen samples were tested using both air and nitrogen gas as pressurants but did not use a corresponding liquid to have surface tension forces of the liquid-vapor interface inside the screen drive screen deflection. Instead, the screen sample was reported to be tested using a technique that clamped both the screen and a thin piece of plastic sheathing together to prevent pressurant from flowing through the screen. The thin plastic sheathing is what created the pressure difference across the screen to induce deflection. It is also what allowed pressure differences across the screen to exceed bubble point pressure. Paynter also reported differences in data due to clamping techniques. The flat clamping technique is reported to have given nonrepeatable results due to "initial sag and waviness" in the screen samples, while a beveled ring design was able to achieve a pretension in the screen sample and produce repeatable results. It was reported that the level of pretension caused by the beveling technique did not have a significant effect on test results. There is a concern that using the plastic sheathing pressurizing technique may have created differences in results that may not reflect screen compliance via surface tension forces. Furthermore, the data reported deflection values at the middle of the screen and does not relate the results to an effective deflection across the screen. Therefore, data from this study will not be used in model development.

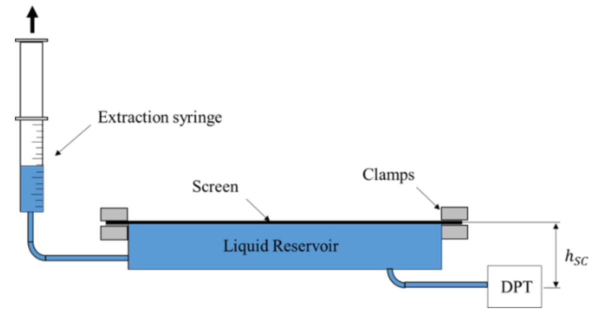

Fig. 6. Simple schematic of experimental setup used to measure screen compliance using a differential pressure transducer (DPT) for Camarotti et al. 2019 [2], Camarotti et al. 2022 [4], and Vasireddy et al. 2022 [5].

Other screen compliance tests have been performed with room temperature fluids using both circular and rectangular screen samples. A simple schematic of the experimental setup used for all three of the following studies is given in Fig. 6. These studies mounted the screen samples into a screen assembly similar to the one shown in Fig. 4.

Camarotti et al. 2019 [2] utilized circular screen samples tested in isopropyl alcohol (IPA) that were mounted using epoxy between two flat shims with no control over pretension. A new equation of state model relating the pressure difference across the screen and the effective thickness of deflection using a constant, K_{SC} (also known as the screen compliance constant), was presented in the Camarotti et al. 2019 study for the linear portion of screen compliance. Note that K_{SC} is defined in the Camarotti et al. 2019 study as the slope for the linear portion of the ΔP_{SC} vs. T_{SC} curve as shown in equation (1). The "Equation of state" section of this paper provides further detail on exactly how K_{SC} is used to couple the conservation of mass and momentum equations via ΔP_{SC} and T_{SC}.

$$\frac{\partial(\Delta P_{SC})}{\partial T_{SC}} = K_{SC} \text{ for linear screen compliance} \quad (1)$$

It was reported in Camarotti et al. 2019 that the K_{SC} value for most screens tested were independent of the open area diameter of the screen assembly for the circular screen samples. As a general weak trend, it was also shown that K_{SC} values increased with increasing screen fineness. A high value of K_{SC} corresponds to less T_{SC} for a given ΔP_{SC}. Since coarse screens tend to be thicker and more rigid than fine screens, it is likely that this trend is a result of the liquid-vapor interface traveling through the thickness of the screen itself, thus inducing a resulting T_{SC} value. Recall that T_{SC} is the effective screen deflection thickness not only caused by the physical bending of the screen, but also the liquid-vapor interface traveling through the screen itself. This point is discussed in further detail by Vasireddy et al. 2022 [5].

Vasireddy et al. 2022 performed a similar study to Camarotti et al. 2019 except rectangular screen samples with varying open area aspect ratios were used. Results from the Vasireddy et al. 2022 study showed that K_{SC} also weakly increased with increasing screen fineness. Due to relatively large uncertainty in reported K_{SC} values of the Vasireddy et al. 2022 study, a definitive trend between aspect ratio and K_{SC} was not achieved. Camarotti et al. 2022 [4] performed similar experiments to Vasireddy et al. 2022 using rectangular screen assemblies, however the focus of the study was on the effects of ramp rate (i.e. liquid withdrawal rate) on screen compliance. It was found that K_{SC} was independent of ramp rates between $0.5 - 16\ ml/min$ for screen samples with open areas of $2'' \times 1''$, $2'' \times 2''$, and $4'' \times 1''$.

The only known publically available analytical model for transient screen compliance of a LAD channel is provided by Jaekle 1997 [1]. While Jaekle does provide some indications on how to solve the model, there is not enough information provided for a complete set of equations (i.e. the equation of state is not given). There is also no derivation or list of assumptions provided for either the mass or the momentum equations, no characteristic speed of the governing equations provided to be used for numerical stability, and no verification study provided for the numerical solver used. No known tool is available to the public to implement this model and simulate transient screen compliance numerically. While Hartwig et al. 2014 [6] and Darr et al. 2017 [7] provided a 1D and 2D steady state model for LAD channel outflow, respectively, the expected screen deflection from outflow transients was not included.

II. PURPOSE

The purpose of this study is to develop and verify a new transient LAD channel screen compliance model. The new model builds upon the previous model by including a viscous term that allows for the steady state pressure drop along the exposed portion of the channel to match the steady state solution provided by Hartwig et al. 2014 [6]. Information is provided on the numerical discretization scheme chosen to solve this model. The numerical discretization will allow for a transient screen compliance computational fluid dynamics (CFD) program to be developed that will give this solution. The stability criteria will be addressed for the numerical discretization scheme used. Data obtained from previous experiments will be used as inputs into this model in order to satisfy the equation of state from Camarotti et al. 2019 [2]. Finally, the solver will be verified via a mesh refinement study, a Generalized Rankine-Hugoniot Condition Analysis, and a comparison with ANSYS Fluent results.

III. MODEL

The original model for transient screen compliance for a LAD channel was provided by Jaekle 1997 [1]. Note that this model only applies to the exposed end of the channel shown in Fig. 2. The fluid element used for this model is given in Fig. 3. Below are the needed assumptions and approximations to solve the transient screen compliance study:

- 1D flow in the x-direction due to negligible flow within the exposed portion of the channel in the y-direction and z-direction (i.e. $u(x,y,z,t) = u(x,t)$)
- Flow is incompressible (i.e. $\rho = constant$)
- Isotropic fluid
- Liquid viscosity is constant for all space and time (i.e. $\mu(x,t) = \mu = constant$)
- Newtonian fluid
- Isothermal fluid
- Gravity is uniform across the channel (i.e. $g = constant$)
- For conservation of mass, an arbitrary stationary deformable control volume is used (i.e. finite control volume analysis used to simplify screen compliance problem into a 1D model)
- For conservation of momentum, a material control volume is used (i.e. differential control volume analysis used assuming screen deflection has a negligible effect on the x-momentum)
- The cross-sectional area of the channel, A_{CH}, is not a function of effective thickness, T_{SC}, (approximation is taken for mass flux terms as part of conservation of mass finite control volume analysis, i.e. $T_{SC} \ll H$)
- K_{SC} values are used for the linear region of screen compliance only (i.e. effects from nonlinear screen compliance are neglected)
- The submerged end of the channel is modeled as quasi-transient flow (i.e. the steady submerged channel solver is updated after each time step)
- The screen compliance constant, K_{SC}, is constant along the length of the channel (i.e. T_{SC} is an effective deflection thickness and not an actual deflection thickness)
- Changes in the amount of liquid above the submerged end of the screen are neglected (i.e. $L_{submerged}$ is a constant over time)

A. Conservation of mass

Due to the assumption that a deformable control volume is to be used for the conservation of mass, the derivation begins with the integral form of the governing equation for an arbitrary stationary control volume as shown in equation (2). In other words, for the conservation of mass equation, a finite control volume analysis is used to create a simple 1D model for this screen compliance problem.

$$\frac{d}{dt}\iiint_{CV} \rho dV + \iint_{CS} \rho \bar{v} \cdot \hat{n} dA = 0 \tag{2}$$

For a 1D incompressible flow in a deformable fixed control volume, equation (3) can be derived using the nomenclature outlined for the control volume in Fig. 3.

$$\rho \frac{\partial V(t)}{\partial t} - \rho u A_{CH} + \rho\left(u + \frac{\partial u}{\partial x}\delta x\right) A_{CH} = 0 \tag{3}$$

where

$$\begin{gathered} V(t) = [H - T_{SC}(t)] w_{SC} \delta x \\ \Rightarrow \frac{\partial V(t)}{\partial t} = -w_{SC} \delta x \frac{\partial T_{SC}}{\partial t} \end{gathered} \tag{4}$$

Note here that in equation (3), the cross sectional area of the channel, A_{CH}, is assumed to be independent of the effective deflection thickness of the screen, T_{SC}, for the mass flux terms into and out of the control volume. However, the deformable (i.e. time dependent) control volume does use T_{SC} in the derivation. This is an implicit approximation that is outlined here for clarity. Now, inserting equation (4) in equation (3) gives the final form of the continuity equation, as shown in equation (5).

$$\begin{gathered} -w_{SC} \delta x \frac{\partial T_{SC}}{\partial t} + \frac{\partial u}{\partial x} \delta x A_{CH} = 0 \\ \Rightarrow \frac{\partial T_{SC}}{\partial t} = \frac{A_{CH}}{w_{SC}} \frac{\partial u}{\partial x} \end{gathered} \tag{5}$$

B. Conservation of momentum

The derivation for the conservation of momentum for screen compliance begins with the Navier-Stokes momentum equation [8]. In other words, for the conservation of momentum equation, a differential (i.e. infinitesimally small) control volume analysis is used to create a simple 1D model for this screen compliance problem. Note that T_{ij} in equation (6) is defined as the stress tensor.

$$\rho \frac{\partial u_j}{\partial t} + \rho u_i \frac{\partial u_j}{\partial x_i} = \rho g_j + \frac{\partial}{\partial x_i}(T_{ij}) \tag{6}$$

Applying the assumption of 1D flow in the x-direction for a laminar incompressible flow, the stress tensor in the momentum equation can be expanded to give equation (7). Note that this 1D approximation implicitly states that the screen deflection does not significantly contribute to x-momentum.

$$\frac{\partial u}{\partial t} + u\frac{\partial u}{\partial x} = -\frac{1}{\rho}\frac{\partial \Delta P_{SC}}{\partial x} - g\frac{\partial z}{\partial x} + \nu \frac{\partial^2 u}{\partial x^2} \tag{7}$$

As a brief aside, note that ΔP_{SC} is used here to indicate a pressure difference between the inside and outside of the LAD channel (i.e. across the screen) as defined in equation (8). For a LAD outflow condition, the ΔP_{SC} value will be negative along the channel (i.e. the pressure inside the channel will be lower than the pressure outside the channel). Since the bubble point, ΔP_{BP}, is defined as the gas side pressure minus the liquid side pressure (i.e. pressure outside the channel minus the pressure inside the channel) across the screen at breakdown as shown in equation (9), the negative value of ΔP_{SC} will need to be taken to make this comparison. For clarity, a new value of $\Delta P_{SC}{}'$ will be defined to make this distinction as shown in equation (10). It is important to note this distinction since historical steady state LAD outflow models [7] [9] have provided steady state solutions for $P_{channel}$ that also need to be manipulated to compare with ΔP_{BP}.

$$\Delta P_{SC} \equiv P_{channel} - P_0 \tag{8}$$

$$\Delta P_{BP} \equiv P_{gas} - P_{liq} = P_0 - P_{channel} \quad @ \text{ breakdown} \tag{9}$$

$$\Delta P_{SC}{}' \equiv -\Delta P_{SC} = P_0 - P_{channel} \tag{10}$$

A variable z is introduced to indicate the height relative to the body force acceleration vector (i.e. gravity) in order to account for hydrostatic pressure differences across the screen along the channel as shown in Fig. 1. The $g\frac{\partial z}{\partial x}$ term is zero if the channel is in a terrestrial horizontal configuration or in a zero-gravity environment. It is important to note the direction of the gravitational acceleration vector, g, in Fig. 1. A negative sign is added in front of the gravitational body force term in the momentum equation to account for the signing convention of ΔP_{SC}. Since ΔP_{SC} indicates the pressure inside the channel minus the pressure outside the channel, the hydrostatic contribution to ΔP_{SC} increases as the liquid level in the tank lowers. The hydrostatic term only applies to the exposed section of the channel since there is no hydrostatic contribution to ΔP_{SC} in the submerged portion of the channel. In other words, if the tank is in a 1-g condition (e.g. a terrestrial environment) for the scenario illustrated in Fig. 1, the signing convention on the gravitational term for equation (7) would require an input of $g = +9.81\ m/s^2$, assuming the z vector is positive.

The form of the momentum equation given in equation (7) is further simplified in the original model to give equation (11). It can be seen that ΔH is used instead of ΔP_{SC} to indicate a pressure difference across the screen between the inside and outside of the channel. The gravitational acceleration, g, is also substituted as a_{SC} to indicate the acceleration vector for a broader source of body forces on the liquid inside the channel (e.g. sudden acceleration or deceleration during docking, centrifugal force, etc.).

The final point of discussion on the original model is the viscous term. The original model used a term that is similar to Poiseuille flow in a constant area channel as shown in equation (11). Although this is not explicitly stated in the 1997 paper [1], the viscous term used here is the same as the viscous term used in Jaekle's 1991 Vanes paper [10] where it is described as modeling "steady, fully developed, laminar flow in a constant area conduit".

$$\frac{\partial u}{\partial t} = -\left(u\frac{\partial u}{\partial x} + \frac{1}{\rho}\frac{\partial(\Delta H)}{\partial x} + a_{SC}\frac{\partial z}{\partial x} + 2\nu\left(\frac{s_{SC}}{A_{CH}}\right)^2 u \right) \tag{11}$$

During the course of this study, it was found that the viscous terms for both equation (7) and equation (11) do not allow for the steady state pressure drop along the exposed portion of the channel to match the steady state solution provided by Hartwig et al. 2014 [6]. In order to account for the steady state viscous pressure drop along the channel in this model, the steady state frictional term from equation (35) in [6] is implemented in this solver. Implementation of this term involves taking the derivative of the frictional pressure drop with respect to x and dividing by the density, ρ. The result from this manipulation is given in equation (12).

$$\frac{1}{\rho}\left(\frac{\partial \Delta P_{SC}}{\partial x}\right)_{frictional} = \frac{u w_{SC} H}{\rho}\left\{\frac{H^3 w_{SC}}{12\mu} + \sum_{n=0}^{\infty}\frac{16}{\mu H \lambda_n^5}\tanh\left(\frac{w_{SC}\lambda_n}{2}\right)\right\}^{-1} + \frac{u^2\left(H + w_{SC}\right)}{16 w_{SC} H\left(\log\left(\frac{14.8 w_{SC} H}{d_s (w_{SC} + H)}\right)\right)^2} \quad (12)$$

The modified form of the momentum equation used in the LAD transient screen compliance solver (prior to coupling to mass via equation of state) is given in equation (13). Note that viscous pressure loss along the channel is considered third order under terrestrial conditions and second order under microgravity conditions [6]. A more detailed discussion on this point will be provided in the "General Discussion" section.

$$\frac{\partial u}{\partial t} = -\left(u\frac{\partial u}{\partial x} + \frac{1}{\rho}\frac{\partial \Delta P_{SC}}{\partial x} + g\frac{\partial z}{\partial x} + \frac{1}{\rho}\left(\frac{\partial \Delta P_{SC}}{\partial x}\right)_{frictional}\right) \quad (13)$$

C. Equation of state

The equation of state relationship shows that the pressure head across the screen is a function of ΔP_{BP}, T_{SC}, and T_{SC_0} as shown in equation (14). Camarotti et al. 2019 [2] developed a relationship between thickness and pressure head given in equation (15) that holds when $\Delta P_{SC}' < \Delta P_{BP}$. This relationship assumes that the screen is completely flat at rest with no initial deflection (i.e. $T_{SC_0} = 0$) and that the deflected thickness is a volume average over the open area of the screen (i.e. T_{SC} is an effective thickness). If there is an interest to only model the linear portion of screen compliance (see Fig. 5), then the $\frac{\partial(\Delta P_{SC})}{\partial T_{SC}}$ term can be set to a constant as shown in equation (1) and the modified equation of state proposed by Camarotti et al. 2019 [2] simplifies to equation (16).

$$\frac{\partial\left(\Delta H\right)}{\partial x} = \frac{\partial}{\partial x}\left(f\left(\Delta P_{BP}, T_{SC}, T_{SC_0}\right)\right) \quad (14)$$

$$\Delta H = \Delta P_{SC} = \frac{V_{SC}}{A_{SC}}\frac{\partial(\Delta P_{SC})}{\partial T_{SC}} = T_{SC}\frac{\partial(\Delta P_{SC})}{\partial T_{SC}} \quad (15)$$

$$\Delta H = \Delta P_{SC} = T_{SC} K_{SC} \quad (16)$$

D. Conservative form of governing equations

Prior to presenting the conservative form of the governing equations, the equation of state given in equation (13) and the conservation of x-momentum given in equation (16) must first be combined so that only two equations and two unknowns remain. The result of combining the x-momentum equation and the equation of state is given in equation (17). The difference in signing convention between the equation of state and the conservation of x-momentum for ΔP_{SC} is accounted for in this equation (i.e. a negative sign is introduced in front of the $\frac{K_{SC}}{\rho}\frac{\partial T_{SC}}{\partial x}$ term).

$$\frac{\partial u}{\partial t} = -\left(u\frac{\partial u}{\partial x} - \frac{K_{SC}}{\rho}\frac{\partial T_{SC}}{\partial x} + g\frac{\partial z}{\partial x} + \frac{1}{\rho}\left(\frac{\partial \Delta P_{SC}}{\partial x}\right)_{frictional}\right) \quad (17)$$

The equation for conservation of mass (i.e. equation (5)) and the combined equation for conservation of momentum and the equation of state (i.e. equation (17)) will now be presented in conservative form. A set of equations in conservative form follows equation (18). The resulting equations for the conserved variable vector, $\vec{U}$, and the flux vector, $\vec{F}$, are given in equation (19) and equation (20) , respectively. The viscous term is treated as a source term, $\vec{S}$, as shown in equation (21). The conservative form of the transient screen compliance governing equations is provided for numerical discretization and further characterization of this set of equations.

$$\frac{\partial \vec{U}}{\partial t} + \frac{\partial \vec{F}}{\partial x} = \vec{S} \quad (18)$$

$$\vec{U} = \begin{bmatrix} T_{SC} \\ u \end{bmatrix} \quad (19)$$

$$\vec{F} = \begin{bmatrix} -\frac{A_{CH}}{w_{SC}} u \\ \frac{1}{2}u^2 - \frac{K_{SC}}{\rho} T_{SC} + gz \end{bmatrix} \quad (20)$$

$$\vec{S} = \begin{bmatrix} 0 \\ -\frac{1}{\rho}\left(\frac{\partial P}{\partial x}\right)_{frictional} \end{bmatrix} \quad (21)$$

E. Characteristic speed

The characteristic speed of the governing equations is provided not only for numerical discretization stability purposes, but also for a better understanding of the behavior of the governing equations. The first step in determining the characteristic speed of the governing transient screen compliance equations is to convert the conservative form of the equations to the form shown in equation (22). In this form, $\bar{\bar{A}}$ is the Jacobian matrix of the flux vector as shown in equation (23). After the Jacobian matrix of the flux vector is found, the eigenvalues of the Jacobian matrix are presented. These eigenvalues, $\lambda^{\pm}$, give the characteristic speed, $u_{characteristic}$, of the governing equations as shown in equation (24).

$$\frac{\partial \bar{U}}{\partial t}+\frac{\partial \bar{F}}{\partial \bar{U}}\frac{\partial \bar{U}}{\partial x}=\vec{S}\ \rightarrow\ \frac{\partial \bar{U}}{\partial t}+\bar{\bar{A}}\frac{\partial \bar{U}}{\partial x}=\vec{S} \quad (22)$$

$$\bar{\bar{A}}=\frac{\partial \bar{F}}{\partial \bar{U}}=\begin{bmatrix} 0 & -\frac{A_{SC}}{w_{SC}} \\ -\frac{K_{SC}}{\rho} & u \end{bmatrix} \quad (23)$$

$$u_{characteristic}=\lambda^{\pm}=\frac{1}{2}\left(u\pm\sqrt{u^2+4\frac{K_{SC}}{\rho}\frac{A_{SC}}{w_{SC}}}\right) \quad (24)$$

F. Initial condition and boundary conditions

1. Initial condition

For the 1D transient screen compliance model, an initial condition of a quiescent fluid with no initial screen deflection is chosen. In other words, $u(x,t=0)=0\ m/s$ and $T_{SC}(x,t=0)=0\ m$ everywhere along the channel (both the exposed and submerged portions of the channel). Using the equation of state, this also implies that $\Delta P_{SC}(x,t=0)=0\ Pa$ everywhere along the channel. Note that this initial condition only applies to a zero-gravity case or a horizontally oriented channel.

For a vertically oriented channel with gravity applied, the velocity, u, will still be zero across the channel initially; however, the T_{SC} and ΔP_{SC} values will initially be a function of x for the exposed portion of the channel. The transient screen compliance solver accounts for this by first calculating the hydrostatic head contribution to ΔP_{SC} and converting it into a T_{SC} initial condition via the equation of state prior to entering the transient numerical scheme. For most of the analysis in this study, gravity will be set to zero to isolate effects from transient screen compliance.

2. Demand end boundary condition ($x = L_{demand}$)

The velocity boundary condition at the demand end of the channel, $u(x=L_{demand},t)$, is a user input as a function of time. The velocity at this boundary is set by the valve opening profile as a function of time. The current transient screen compliance solver allows for the user to input a linear, step change, equal percentage or quick valve opening. A graphical example of the linear, quick opening and equal percentage profiles is given in Fig. 7. The corresponding equations used for these profiles is given in equation (25) through equation (27), respectively. In these equations, u_{demand} is the steady state demand velocity and t_{open} is the time when the valve is fully open (i.e. valve opening time). Note that the step change valve opening profile simply sets $u(x=L_{demand},t)=u_{demand}$ for $t>0\ sec$.

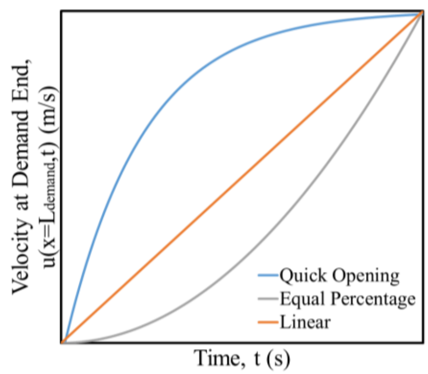

Fig. 7. Graphical example of valve opening profiles used as inputs for the demand end of the channel.

Linear Profile:

$$u(x=L_{demand},t)=\begin{cases} u_{demand}\dfrac{t}{t_{open}} & if\ \ t<t_{open} \\ u_{demand} & if\ \ t\geq t_{open} \end{cases} \quad (25)$$

Quick Opening Profile:

$$u(x=L_{demand},t)=u_{demand}\left(1-\exp\left(\ln(0.01)\left(\frac{t}{t_{open}}\right)\right)\right) \quad (26)$$

Equal Percentage Profile:

$$u(x=L_{demand},t)=\begin{cases} u_{demand}\left(\dfrac{t}{t_{open}}\right)^2 & if\ \ t<t_{open} \\ u_{demand} & if\ \ t\geq t_{open} \end{cases} \quad (27)$$

The thickness boundary condition at the demand end of the channel, $T_{SC}(x=L_{demand},t)$, is extrapolated from the adjacent interior node point (i.e. $\left.\frac{\partial T_{SC}}{\partial x}\right|_{x=L_{demand}}=0$ occurs locally between the demand boundary and adjacent interior node). Referencing the equation of state, this implicitly states that the pressure difference across the screen along the channel, ΔP_{SC}, does not change between the demand end boundary node and the node adjacent to the demand end boundary node (i.e. zero-order extrapolation). The error introduced from this approximation approaches zero as the grid spacing goes to zero.

Originally, it was thought that T_{SC} would need to be set to zero at the demand end boundary since the screen is fixed at that location. After further consideration, it was found that this would not make sense physically since it would also set ΔP_{SC} equal to zero at that location via the equation of state. The reason why T_{SC} can be nonzero at the fixed demand end boundary is because T_{SC} is not an actual deflection thickness, but rather an effective deflection thickness. Recall that T_{SC} was originally derived in Camarotti et al. 2019 [2] by simply taking the volume of liquid extracted from the experimental screen compliance reservoir and dividing it by the area of the screen, A_{SC}. This methodology does not account for the exact profile of screen deflection, thus creating an effective deflection thickness.

3. Submerged end boundary condition ($\boldsymbol{x = L_{submerged}}$)

The velocity boundary condition at the submerged end of the channel, $u(x = L_{submerged}, t)$, is extrapolated from the adjacent interior node point (i.e. $\left.\frac{\partial u}{\partial x}\right|_{x=L_{submerged}} = 0$ occurs locally between the submerged boundary and adjacent interior node). This implicitly states that the x-velocity does not change between the submerged end boundary node and the node adjacent to the submerged end boundary (i.e. zero-order extrapolation). The error introduced from this approximation approaches zero as the grid spacing goes to zero.

There are two methods that are recommended to address the effective deflection thickness at the submerged end boundary condition, $T_{SC}(x = L_{submerged}, t)$, for each time step. The first method (referred to as Method 1) involves taking the velocity boundary condition at the submerged end of the channel, $u(x = L_{submerged}, t)$, and inputting it into the steady 2D channel outflow solver which is based off of the equations from Darr et al. 2017 [7] (outlined in the "Steady State Model" subsection). From this steady 2D channel outflow solver, a pressure difference across the screen is determined at the submerged end of the channel, $\Delta P_{SC}(x = L_{submerged}, t)$. The resulting ΔP_{SC} is converted to T_{SC} using the equation of state, thus establishing the boundary condition for effective deflection thickness at the submerged end of the channel, $T_{SC}(x = L_{submerged}, t)$. The 2D channel outflow solver is implemented for each time step within the transient screen compliance solver. This is how the transient 1D solver for the exposed end of the channel is coupled to the steady 2D outflow solver for the submerged end of the channel. Note that Method 1 does not assume a uniform injection velocity across the screen for the submerged end of the channel.

The second method (referred to here as Method 2) involves taking the velocity boundary condition at the submerged end of the channel, $u(x = L_{submerged}, t)$, and inputting it into the Armour and Cannon flow through screen pressure drop, ΔP_{FTS}, model [11]. Method 2 is performed by converting the mass flow at $x = L_{submerged}$ to an evenly distributed injection velocity across the entire submerged portion of the channel. This approach is analogous to what was performed for the Hartwig et al. 2014 1D steady outflow model [6]. The equations used from Hartwig et al. 2014 are outlined in the "Steady State Model" subsection.

For most of the analysis for in this study, Method 1 will be used. However, it was decided to use Method 2 for a comparison of transient screen compliance solver results to ANSYS Fluent results due to the ease of implementation of this method. Note that Method 1 and Method 2 produce similar results for low demand Reynolds numbers (i.e. the submerged injection profile is uniform for low demand Reynolds numbers).

G. Steady state model

The steady state model used for the pressure drop across the screen for the exposed portion of the LAD channel ($\Delta P_{SC,SS,exposed}$) has been previously developed by Hartwig et al. 2014 [6]. The $\Delta P_{SC,SS,exposed}$ in this model is separated into four terms: hydrostatic pressure drop ($\Delta P_{hydrostatic}$), flow through screen pressure drop (ΔP_{FTS}), frictional pressure drop ($\Delta P_{frictional}$), and dynamic pressure drop ($\Delta P_{dynamic}$). For this study, the steady state model from Hartwig et al. 2014 is applied to the exposed section of the channel; therefore, the ΔP_{FTS} term does not apply here. Furthermore, the $\Delta P_{dynamic}$ is accounted for in the submerged section steady state solver and does not need to be double counted in the exposed section of the channel.

For convenience, the $\Delta P_{SC,SS,exposed}$ model used for the exposed portion of the channel is given in equation (28) through equation (30). In these equations, x is the dimension along the length of the channel, $L_{submerged}$ is the submerged length of the channel, and u_{demand} is the steady state demand velocity. For the exposed portion of the screen, $\Delta P_{SC,SS,exposed}$ can be converted to an effective deflection thickness at steady state ($T_{SC,SS,exposed}$) by simply imposing the equation of state and accounting for the appropriate signing convention.

$$\Delta P_{SC,SS,exposed} = \Delta P_{SC,SS,submerged} - \Delta P_{hydrostatic} - \Delta P_{frictional} \tag{28}$$

$$\Delta P_{hydrostatic} = \rho g (x - L_{submerged}) \tag{29}$$

$$\begin{aligned}\Delta P_{frictional} &= u_{demand} w_{SC} H (x - L_{submerged}) \left\{ \frac{H^3 w_{SC}}{12\mu} + \sum_{n=0}^{\infty} \frac{16}{\mu H \lambda_n^5} \tanh\left(\frac{w_{SC}\lambda_n}{2}\right) \right\}^{-1} \\ &+ \frac{\rho u_{demand}{}^2 (x - L_{submerged})(H + w_{SC})}{16 w_{SC} H \left(\log\left(\frac{14.8 w_{SC} H}{d_s (w_{SC} + H)} \right) \right)^2}\end{aligned} \tag{30}$$

The $\Delta P_{SC,SS,submerged}$ terms to be evaluated when Method 1 (i.e. Darr et al. 2017 [7]) is applied is given in equation (31) through equation (35). In these equations, a fourth order Runge-Kutta method combined with the shooting method is used to solve for f which is then used to find $\Delta P_{SC,SS,submerged}$. In these equations, α and β are the Armour and Cannon fitting coefficients, Q is the tortuosity factor, B is the thickness of the screen, a is the surface area to volume ratio of the screen, ε is the screen porosity, D_P is the effective pore diameter of the screen, and v_{inj} is the injection velocity into the channel across the screen.

Method 1:

$$\left(\frac{1}{\mathrm{Re}_e} + \frac{N_{lam}}{\mathrm{Re}_e} + 2C_{turb} f' \right) f'' - \frac{12}{\mathrm{Re}_e}(1+f) - \frac{12}{5} f'(1+f) = 0 \tag{31}$$

$$\mathrm{Re}_e = \frac{\rho u_{demand} H}{\mu} \;,\; N_{lam} = C_{lam} H \tag{32}$$

$$v_{inj} = -u_{demand} f' \tag{33}$$

$$C_{lam} = \alpha \left(\frac{QBa^2}{\varepsilon^2} \right) \;,\; C_{turb} = \beta \left(\frac{QB}{\varepsilon^2 D_P} \right) \tag{34}$$

$$\Delta P_{SC,SS,submerged} = -\left(C_{lam} \mu \left| v_{inj} \right| + C_{turb} \rho v_{inj}{}^2 \right) \tag{35}$$

The $\Delta P_{SC,SS,submerged}$ terms to be evaluated when Method 2 (i.e. Hartwig et al. 2014 [6]) is applied is given in equation (36) through equation (38). In these equations, $\dot{m}$ is the demand mass flow rate and A_{SC} is the cross-sectional area of the screen. Note here that the ΔP_{FTS} and $\Delta P_{dynamic}$ terms are included and the $\Delta P_{hydrostatic}$ term is removed for the submerged case.

Method 2:

$$\Delta P_{SC,SS,submerged} = -\Delta P_{dynamic} - \Delta P_{frictional} - \Delta P_{FTS} \tag{36}$$

$$\Delta P_{FTS} = \alpha \left(\frac{QB\mu a^2}{\rho \varepsilon^2} \right) \left(\frac{\dot{m}}{A_{SC}} \right) + \beta \left(\frac{QB}{\rho \varepsilon^2 D_P} \right) \left(\frac{\dot{m}}{A_{SC}} \right)^2 \tag{37}$$

$$\Delta P_{dynamic} = \frac{\dot{m}^2}{2\rho H^2 w_{SC}{}^2} \tag{38}$$

For the exposed portion of the channel (i.e. $L_{submerged} < x < L_{demand}$), the steady state x-component of the velocity ($u_{SS,exposed}$) is simply equal to u_{demand}. The reason for this is that at steady state, the exposed section of the channel is essentially a constant area rectangular duct with an incompressible fluid flowing through it. Therefore, to satisfy continuity at steady state, $u_{SS,exposed}(x, t \to \infty) = u_{demand}$. For the submerged portion of the channel (i.e. $0 < x < L_{submerged}$), the value for the steady state x-component of the velocity ($u_{SS,submerged}$) depends on whether Method 1 or Method 2 is used. If Method 1 is chosen, then equation (39) can be used to find $u_{SS,submerged}$. Note that this is the average of the u velocity profile defined in Darr et al. 2017 [7]. In this equation, f is solved for in the same manner discussed previously. If Method 2 is chosen, then equation (40) can be used to find $u_{SS,submerged}$. In this equation, v_{inj} is first found using a mass balance for the submerged portion of the channel assuming a uniform injection profile as shown in equation (41). Since Method 2 assumes a uniform injection velocity profile, a simple differential element mass balance can be performed on the submerged portion of the channel to find $u_{SS,submerged}$ shown in equation (40).

Method 1:

$$u_{SS,submerged} = \frac{1}{H} \int_0^H u_{demand} (1+f) \left(6 \frac{y}{H} \left(1 - \frac{y}{H} \right) \right) dy \tag{39}$$

Method 2:

$$u_{SS,submerged} = v_{inj} \frac{x}{H} \tag{40}$$

Method 2:

$$v_{inj} = \frac{u_{demand} H}{L_{submerged}} \tag{41}$$

IV. TRANSIENT SCREEN COMPLIANCE SOLVER

A. Numerical discretization

The numerical scheme used in the transient screen compliance solver is the Two-Step Lax-Wendroff method of Rubin and Burstein 1967 [12]. The first step for this method is given in equation (42) and involves calculating velocity and thickness values at half spatial steps and full timesteps via averaging. The second step in the method is given by equation (43). The definition for the half steps of the flux vector is given in equation (44). The values for $\vec{U}$, $\vec{F}$, and $\vec{S}$ are given in equation (19), equation (20), and equation (21), respectively.

$$\begin{aligned} U_{i+\frac{1}{2}}^{\overline{n+1}} &= \frac{1}{2}\left(U_i^n + U_{i+1}^n\right) - \Delta t\left[\frac{F_{i+1}^n - F_i^n}{\Delta x}\right] \\ U_{i-\frac{1}{2}}^{\overline{n+1}} &= \frac{1}{2}\left(U_i^n + U_{i-1}^n\right) - \Delta t\left[\frac{F_i^n - F_{i-1}^n}{\Delta x}\right] \end{aligned} \tag{42}$$

$$U_i^{n+1} = U_i^n - \Delta t\left\{\frac{1}{2}\left[\frac{F_{i+1}^n - F_{i-1}^n}{2\Delta x} + \frac{F_{i+\frac{1}{2}}^{\overline{n+1}} - F_{i-\frac{1}{2}}^{\overline{n+1}}}{\Delta x}\right]\right\} + \Delta t S_i^n \tag{43}$$

$$F_{i\pm\frac{1}{2}}^{\overline{n+1}} = F\left(U_{i\pm\frac{1}{2}}^{\overline{n+1}}\right) \tag{44}$$

B. Stability criteria

For all finite difference numerical discretization methods (e.g. Two-Step Lax-Wendroff method of Rubin and Burstein), stability criteria must be established to avoid unbounded growth of the solution in time. In many classical stability definitions, a Courant-Friedrichs-Lewy (CFL) number limit is established so that a Δt can be found for a given Δx used in the numerical scheme. If a Δt is used that causes the CFL stability limit to be exceeded, the solution will experience unbounded growth in time and diverge.

The stability criteria for this scheme is broken up into two components: inviscid stability, and viscid stability. It is common to split the nonlinear inviscid component and the linear viscid component of the governing equations to determine stability for finite difference methods. The inviscid stability deals with the characteristic speed of the inviscid set of equations as defined in the previous section. The viscid stability deals with only the viscous term. A CFL number will be determined for each component and a value of dt will be chosen based on the stricter requirement (i.e. inviscid or viscid). Note that the definition for viscous stability is based on a classical second derivative definition of the viscous term; however, this classical viscous term is not used in the governing equations of this study. Nevertheless, the viscous stability definition is kept here out of conservativism to provide an additional layer of Δt requirements to combat stability issues.

Traditionally, a CFL number is determined by multiplying a velocity by a ratio of $\Delta t/\Delta x$. In the Euler equations, the velocity multiplied by the ratio of $\Delta t/\Delta x$ is the characteristic speed of the equations. In the screen compliance equations, since the characteristic speed is different than the Euler equations, the ratio of $\Delta t/\Delta x$will be multiplied by the maximum absolute value of the characteristic speed given in equation (24). The result of this substitution and the corresponding limit of Δt for the inviscid portion of screen compliance is given in equation (45) and equation (46), respectively. The maximum value of $u_{characteristic}$ is used to create a strict stability requirement for the two characteristic speeds. In other words, if the minimum value is taken, the Δt_{invisc} value would be larger which is not conservative (i.e. strict) in terms of stability.

$$\begin{aligned} CFL_{invisc} &= u_{characteristic} \frac{\Delta t_{invisc}}{\Delta x} \\ &= \max \left| u \pm \sqrt{u^2 + \frac{K_{SC}}{\rho} \frac{A_{SC}}{w_{SC}}} \right| \frac{\Delta t_{invisc}}{\Delta x} \end{aligned} \tag{45}$$

$$\Delta t_{invisc} = \frac{(CFL_{invisc})\Delta x}{\max \left| u \pm \sqrt{u^2 + \frac{K_{SC}}{\rho} \frac{A_{SC}}{w_{SC}}} \right|} \tag{46}$$

The viscid CFL-type number follows the traditional definition of kinematic viscosity, ν, multiplied by $\Delta t/(\Delta x^2)$. The equation for this viscid CFL-type number and the corresponding limit of Δt is given in equation (47) and equation (48), respectively.

$$CFL_{visc} = \nu \frac{\Delta t_{visc}}{(\Delta x)^2} \tag{47}$$

$$\Delta t_{visc} = \frac{(CFL_{visc})(\Delta x)^2}{\nu} \tag{48}$$

After performing a series of numerical test cases, Rubin and Burstein [12] suggested that a CFL number of 0.98 should be used to establish the stability limit for Δt. Therefore, a value of 0.98 was used for both the inviscid and viscid stability criteria. To determine a value for CFL_{invisc} and corresponding Δt_{invisc}, the steady state demand velocity, u_{demand}, is used in the transient screen compliance solver prior to entering the numerical scheme. The stricter of the two Δt requirements is then chosen and held constant throughout the numerical solution process to ensure stability.

C. Transient screen compliance solver verification

1. Mesh refinement analysis

A mesh refinement analysis was performed for the transient screen compliance solver to determine a mesh size that yielded a solution that is grid independent and to determine the rate of convergence for the numerical scheme and boundary conditions used. Specifically, grid independence is defined as the mesh size that does not result in a change of results more than 1%. The improvement of results is defined by the error in the average velocity across the exposed section of the screen as a function of time. The error for a given mesh size, $Error_M$, is more clearly defined in equation (49). In this equation, the operator $\|\xi\|$ is the L2-norm (i.e. Euclidean norm), $[u_{avg}]$ is the vector of average velocity across the exposed section of the channel as a function of time, M is the mesh size, and M_{max} is the finest mesh size used as part of this analysis.

$$Error_M = \frac{\left\| \left[u_{avg} \right]_{M_{max}} - \left[u_{avg} \right]_M \right\|}{\left\| \left[u_{avg} \right]_{M_{max}} \right\|} \tag{49}$$

The inputs used for the cases of the mesh refinement analysis are given in Table 1 and Table 2. The graphical outputs from these cases are given in Fig. 8 through Fig. 10. Fig. 8 shows how the scheme converges by displaying $Error_M$ as a function of grid size, Δx. It can be seen from Fig. 8 that the rate of convergence, p, starts around $p = 1$ for the coarsest grids and approaches $p = 2$ as the grid spacing decreases. Fig. 9 displays the average velocity, u_{avg}, across the exposed section of the channel as a function of time for each grid size. Fig. 10 displays the velocity across the entire channel, u, as a function of channel location, x, at a time of $t = 0.05\ s$ for each grid size. Note that Fig. 10 is not used to determine $Error_M$, but is shown for the sake of completeness. From this analysis, it is concluded that Case 4 (i.e. $\Delta x = 2.29 \times 10^{-3}\ m, \Delta t = 1.04 \times 10^{-4}\ s$) displays grid independence in the manner previously defined for the cases studied.

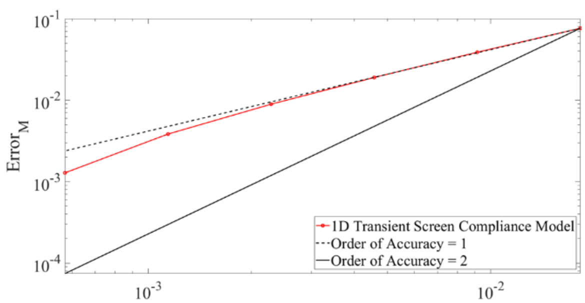

Fig. 8. $Error_M$ as function of grid size for mesh refinement analysis.

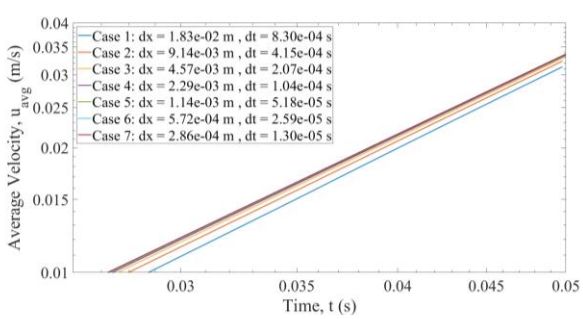

Fig. 9. Average velocity for the exposed end of the channel as function of time for mesh refinement analysis.

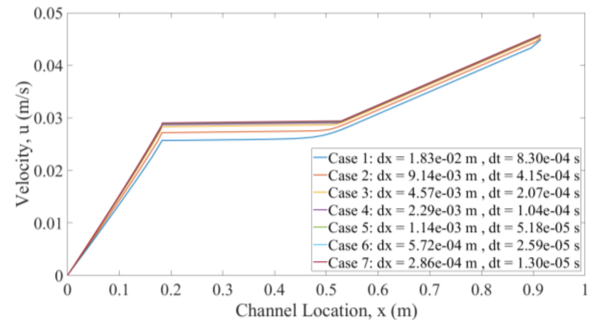

Fig. 10. Velocity as function of channel location at $t = 0.05\ sec$ for mesh refinement analysis.

Table 1. Shared inputs across all cases used in mesh refinement study. Note that fluid properties are evaluated at saturation for the given liquid temperature (i.e. quality of zero) and gravity is set to zero for all cases.

Input	Value
Channel Cross-Sectional Aspect Ratio, w_{SC}/H	4
Channel Cross-Sectional Width, w_{SC} (in)	4
Fluid Type	Methane
Liquid Temperature, T_{liq} (K)	111.6
Liquid Density, ρ (kg/m^3)	422.5
Liquid Viscosity, μ $(Pa \cdot s)$	1.17E-04
Demand Mass Flow, $\dot{m}$ (kg/s)	0.1
Screen Type	200x600
Screen Compliance Constant, K_{sc} (Pa/m)	7.73E+06
Outlet Valve Opening Time, t_{open} (s)	0.1
Profile to Steady State	Linear
Exposed Channel Length Ratio, $L_{exposed}/L$	0.8
Total Channel Length, L (in)	36

Table 2. Number of exposed and submerged grid points used for each mesh refinement case.

Case	Exposed Grid Points	Submerged Grid Points
1	41	11
2	81	21
3	161	41
4	321	81
5	641	161
6	1281	321
7	2561	641

2. *Generalized Rankine-Hugoniot condition analysis*

A Generalized Rankine-Hugoniot (RH) Condition Analysis is performed to verify the numerical scheme used to solve the governing equations of screen compliance for the exposed portion of the channel. For this analysis, an inviscid and zero-gravity case is considered. Note that the Two-Step Lax-Wendroff method of Rubin and Burstein [12] was only used on the convective flux terms, therefore this analysis should be sufficient for verifying the numerical scheme. The simplified case reduces the conservative form of the governing equations as shown in equation (50) through (52).

$$\frac{\partial \bar{U}}{\partial t} + \frac{\partial \bar{F}}{\partial x} = 0 \tag{50}$$

$$\bar{U} = \begin{bmatrix} T_{SC} \\ u \end{bmatrix} \tag{51}$$

$$\bar{F} = \begin{bmatrix} -\dfrac{A_{CH}}{w_{SC}} u \\ \dfrac{1}{2}u^2 - \dfrac{K_{SC}}{\rho} T_{SC} \end{bmatrix} \tag{52}$$

Performing the Generalized RH Condition Analysis involves first defining the RH Condition given below for a traveling Heaviside step function with the corresponding explicit governing equations. Equation (53) is the Generalized RH Condition which is used to write conservation of mass and momentum in equation (54) and equation (55), respectively. In these equations, subscripts L and R correspond to values on the left and right sides of the step function. S is the wave speed of the Heaviside step function. The corresponding schematic for this scenario is given in Fig. 11.

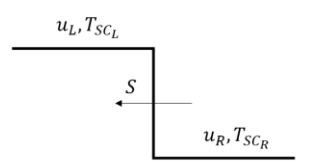

Fig. 11. Simple schematic for Generalized RH Condition Analysis for a traveling Heaviside step function.

$$[F] = S[U] \tag{53}$$

$$-\frac{A_{CH}}{w_{SC}}(u_R - u_L) = S(T_{SC_R} - T_{SC_L}) \tag{54}$$

$$\left(\frac{1}{2}u_R{}^2 - \frac{K_{SC}}{\rho}T_{SC_R}\right) - \left(\frac{1}{2}u_L{}^2 - \frac{K_{SC}}{\rho}T_{SC_L}\right) = S(u_R - u_L) \tag{55}$$

The Generalized RH Condition equations above are solved by picking values for u_L, T_{SC_L}, S and solving for u_R, T_{SC_R}. Solving two equations above for the two unknowns (u_R, T_{SC_R}) gives the relationships for u_R and T_{SC_R} in equation (56) through equation (60). For this analysis, S will be negative (i.e. the wave travels from right to left) as shown in Fig. 11.

$$u_R = \frac{-b_{RH} \pm \sqrt{b_{RH}{}^2 - 4a_{RH}c_{RH}}}{2a_{RH}} \tag{56}$$

$$a_{RH} = \frac{1}{2} \tag{57}$$

$$b_{RH} = \frac{K_{SC}A_{CH}}{S\rho w_{SC}} - S \tag{58}$$

$$c_{RH} = \left(S - \frac{K_{SC}A_{CH}}{S\rho w_{SC}}\right)u_L - \frac{1}{2}u_L{}^2 \tag{59}$$

$$T_{SC_R} = T_{SC_L} - \frac{A_{CH}}{Sw_{SC}}(u_R - u_L) \tag{60}$$

An interesting observation is made on the equations above when $S = \pm\sqrt{\frac{K_{SC}A_{CH}}{\rho w_{SC}}}$. Specifically, setting S to this value results in $u_R = u_L$ and $T_{SC_R} = T_{SC_L}$. Note that if the wave is traveling from right to left (i.e. $S < 0$), a positive sign is used in the quadratic equation for u_R if the magnitude of the wave speed, $|S|$, is less than $\sqrt{\frac{K_{SC}A_{CH}}{\rho w_{SC}}}$, and vice versa. If the wave is traveling from left to right (i.e. $S > 0$), a positive sign is used in the quadratic equation for u_R if the magnitude of the wave speed, $|S|$, is greater than $\sqrt{\frac{K_{SC}A_{CH}}{\rho w_{SC}}}$, and vice versa. Also note that these set of governing equations do not support a standing wave (i.e. $S = 0$).

For this analysis, two different cases are presented with values of S chosen with respect to this interesting value of $S = \pm\sqrt{\frac{K_{SC}A_{CH}}{\rho w_{SC}}}$. Case 1 sets $S = -10^{-6} - \sqrt{\frac{K_{SC}A_{CH}}{\rho w_{SC}}}$ and Case 2 sets $S = -1 - \sqrt{\frac{K_{SC}A_{CH}}{\rho w_{SC}}}$. The behavior of the scheme will be shown for each case with a a grid size of $N = 321$ at various times. Below are the shared inputs used across both cases. The length of the submerged section of the channel is not used as an input for this Generalized RH Condition analysis since the Two-Step Lax-Wendroff method of Rubin and Burstein used for the transient screen compliance solver only applies to the exposed portion of the channel.

- Velocity to the left of the step function, $u_L = 0\ m/s$
- Effective Deflection Thickness to the left of the step function, $T_{SC_L} = 0\ m$
- Density, $\rho = 422.5\ kg/m^3$
- CFL Number = 0.98
- Exposed Channel Length, $L_{exposed} = 0.7315\ m$

- Channel Width, $w_{SC} = 0.1016\ m$
- Channel Area, $A_{CH} = 0.0026\ m^2$
- Screen Compliance Constant, $K_{SC} = 7.73 \times 10^6\ Pa/m$
- $\sqrt{\frac{K_{SC} A_{CH}}{\rho w_{SC}}} = 21.558423\ m/s$

Results for Case 1 and Case 2 are shown in Fig. 12 and Fig. 13, respectively, with a grid size of $N = 321$. Note that the results are compared to an exact solution that has a wave speed equal to the chosen value of S and a wave magnitude equal to the calculated value of u_R and T_{SC_R} for each case. The numerical overshoot shown in the scheme is expected for the Two-Step Lax-Wendroff method being used. This numerical overshoot should not be a major issue in the screen compliance problem since the valve opening time is finite (i.e. valve opening time, $t_{open} > 0$). Therefore, the exposed end of the channel will not experience a large discontinuity resembling what is used in this Generalized RH Condition Analysis. Furthermore, the numerical overshoot in this case is considered to be conservative since it predicts a higher T_{SC} (and corresponding ΔP_{SC}) when compared to a case with no numerical overshoot. As a result, the implemented Two-Step Lax-Wendroff method of Rubin and Burstein works relatively well for this application.

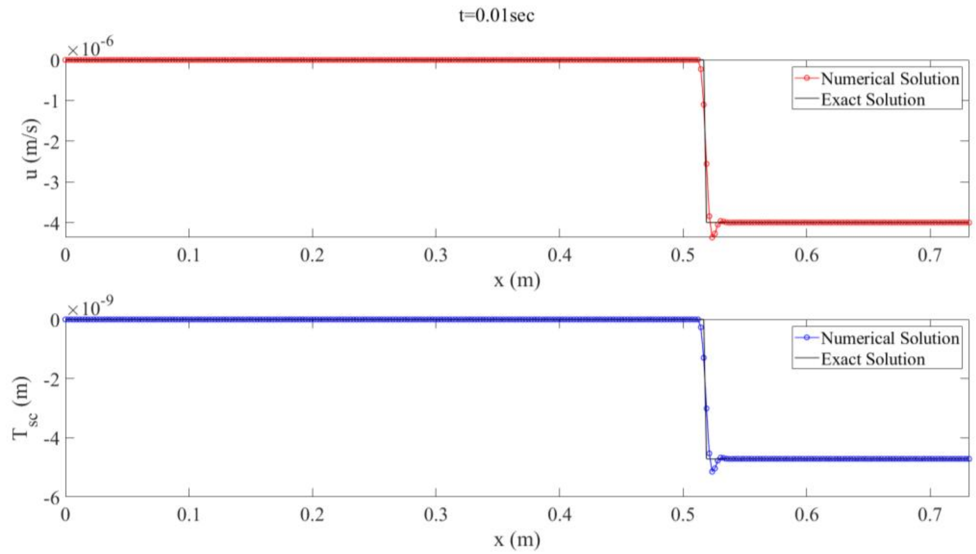

A)

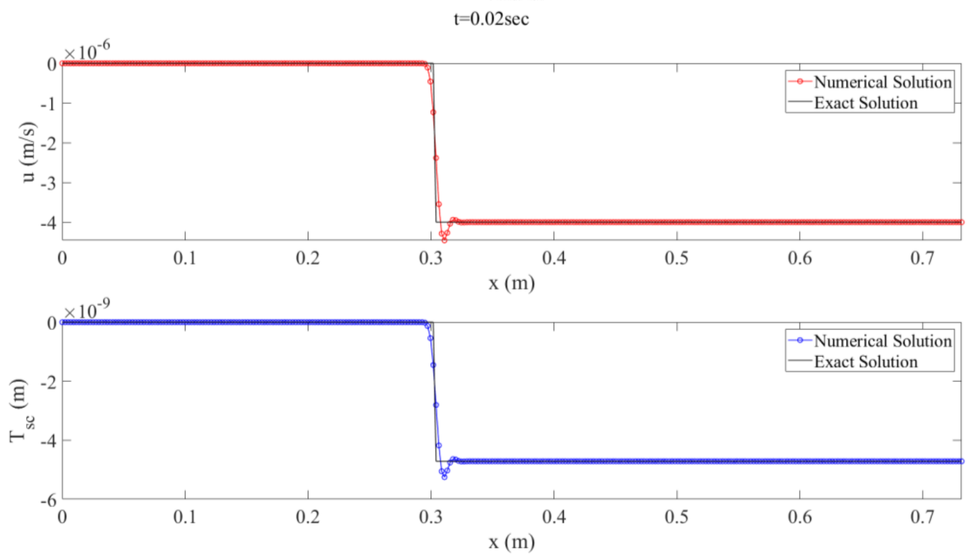

B)

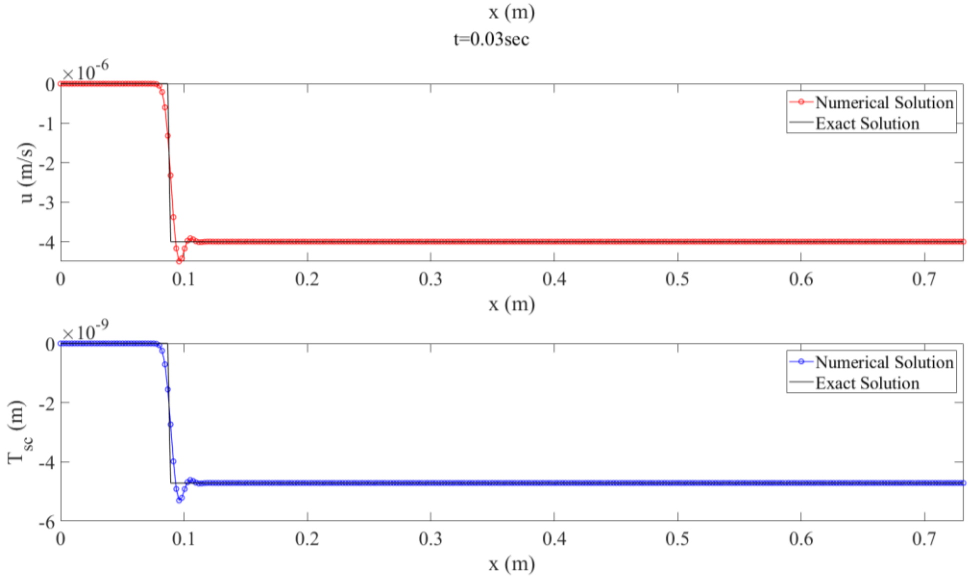

C)

Fig. 12. Results from Case 1 with $S = -10^{-6} - \sqrt{\frac{K_{SC}A_{CH}}{\rho w_{SC}}}$ and $N = 321$ at time A) $t = 0.01\ s$, B) $t = 0.02\ s$, and C) $t = 0.03$.

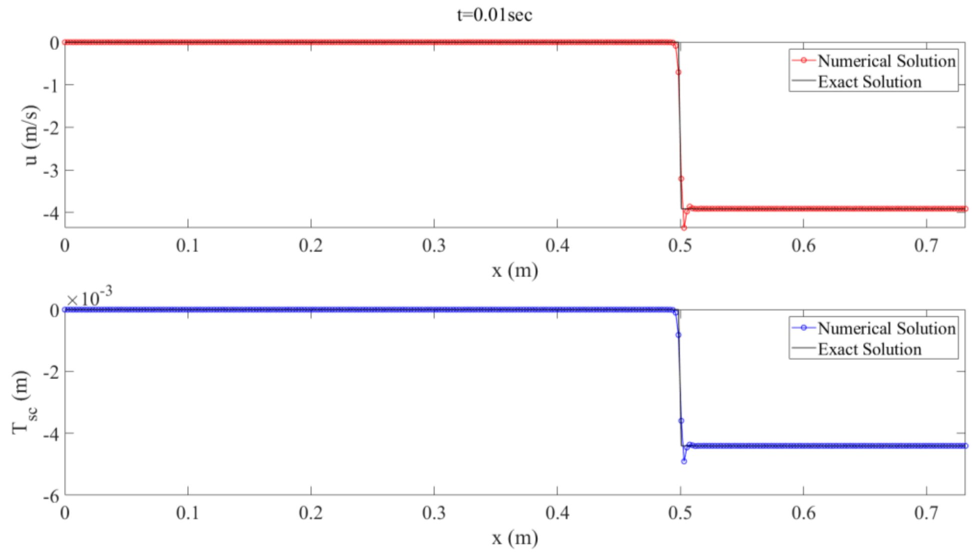

A)

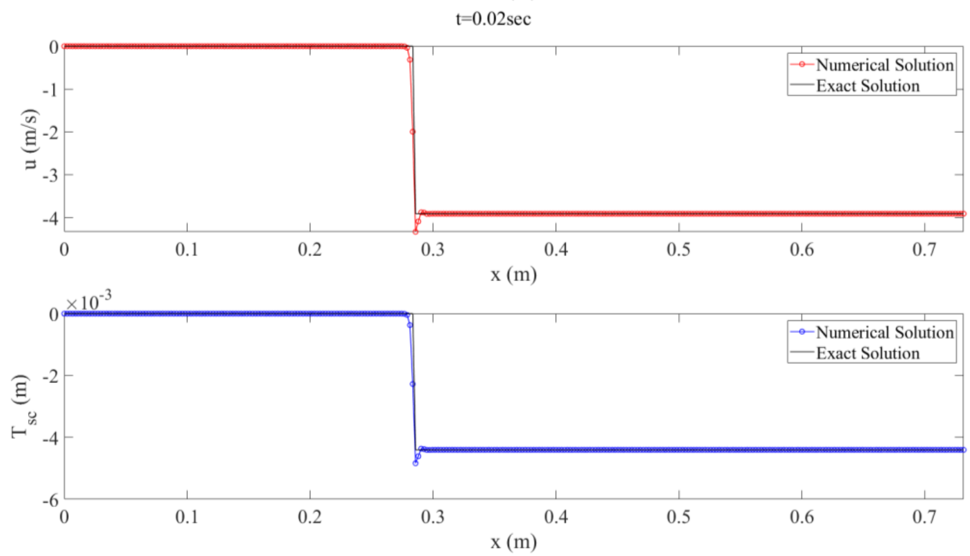

B)

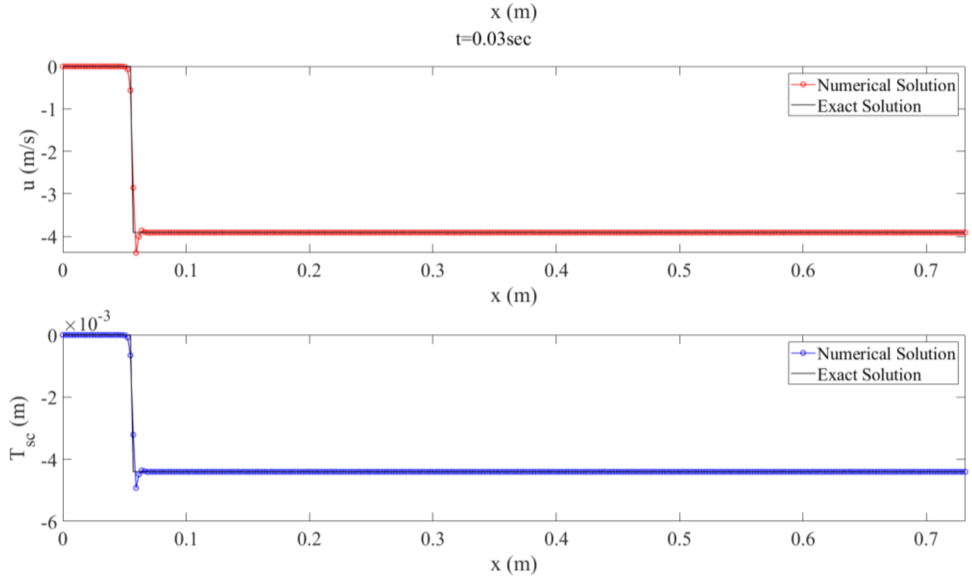

C)

Fig. 13. Results from Case 2 with $S = -1 - \sqrt{\frac{K_{SC}A_{CH}}{\rho w_{SC}}}$ and $N = 321$ at time A) $t = 0.01\ s$, B) $t = 0.02\ s$, and C) $t = 0.03\ s$.

3. Comparison with ANSYS Fluent

In addition to the previously discussed analyses, a comparison was also made between ANSYS Fluent results and the transient screen compliance solver. A comparison to ANSYS Fluent was made for three reasons. First, there is currently no known publically available data for full LAD channel screen compliance, therefore a comparison to ANSYS Fluent is being used as a check (not a full model validation). Second, the transient screen compliance solver and the ANSYS Fluent solver use two different numerical schemes (i.e. finite difference method and finite volume method, respectively) with results showing that major features of the solution are mostly independent of the scheme used. Third, the transient screen compliance solver is 1D and the ANSYS Fluent solver is 2D with results showing that the 1D assumption does not have a significant impact on results.

There are a few important notes to make for this comparison. First, the ANSYS Fluent model uses a pressure-based solver while the transient screen compliance solver uses the Two-step Lax-Wendroff method of Rubin and Burstein. The ANSYS Fluent model utilizes a dynamic mesh that updates after each iteration within a timestep to strongly couple the effective deflection thickness, T_{SC}, and the pressure difference across the screen, ΔP_{SC}. The transient screen compliance solver solves the governing equations of screen compliance explicitly using a non-iterative method.

The second note to make for this comparison is regarding boundary conditions. The boundary conditions at $x = L_{submerged}$ and $x = L_{demand}$ are the same for both models. Since the ANSYS Fluent model is a 2D solver, there are two additional boundary conditions needed for input. The boundary condition at the top of the channel ($y = H$) is determined as follows: pressure is extrapolated from an interior cell center to the boundary face ($\frac{\partial(\Delta P_{SC})}{\partial y}\Big|_{y=} = 0$) and then converted to an effective deflection thickness, T_{SC}, via the equation of state. T_{SC} is then used to dynamically update the mesh after each iteration using a user defined function (UDF). The boundary condition at the bottom of the channel ($y = 0$) is simply modeled as a wall in ANSYS Fluent (i.e. no-slip condition). In other words, for the boundary at the bottom of the channel, $u(y = 0) = 0$.

Third, the 2D ANSYS Fluent model that was used took multiple days to run for a half second transient simulation. This is due to the dynamic mesh updating method and strong under-relaxation factors that were used for the ANSYS Fluent model. To the best knowledge of the author, ANSYS Fluent does not allow for parallel computing to be easily implemented for the dynamic mesh updating tool which drastically increased computation time. For comparison, the hand-written 1D transient screen compliance solver took either a few seconds or minutes to run, depending on the inputs for a given case.

The remaining inputs for the transient screen compliance solver and ANSYS Fluent comparison are given in Table 3. A qualitative comparison between the two solvers can be seen in Fig. 14 for the initiation of the transient. Fig. 15 shows how the transient solutions approach the steady state solution as time increases. Note that in both figures, the steady state solution represents the model that is outlined in the "Steady state model" section.

It can be seen in these figures that the solutions agree well with respect to wave propagation speed and wave magnitude. The discrepancy between the solutions arises when the sharpness of the wave is considered. It is suspected that this is a result of the differences between numerical schemes used in the transient screen compliance and ANSYS Fluent solvers. Fortunately, it appears that the sharpness of the wave does not have an impact on the acceptance criteria of the solver (i.e. maximum pressure difference across the screen, $\Delta P_{SC_{max}}'$).

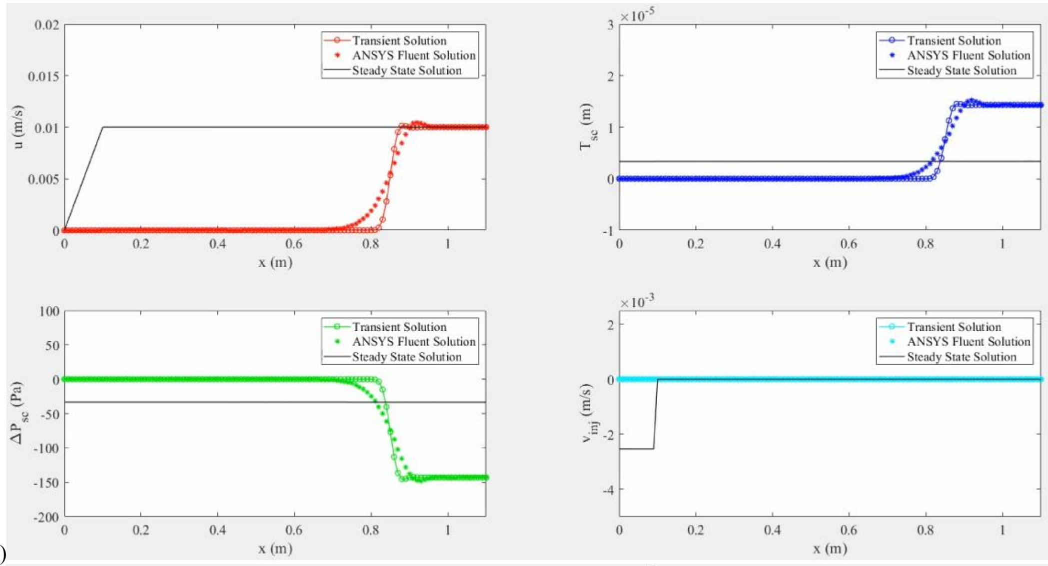

A)

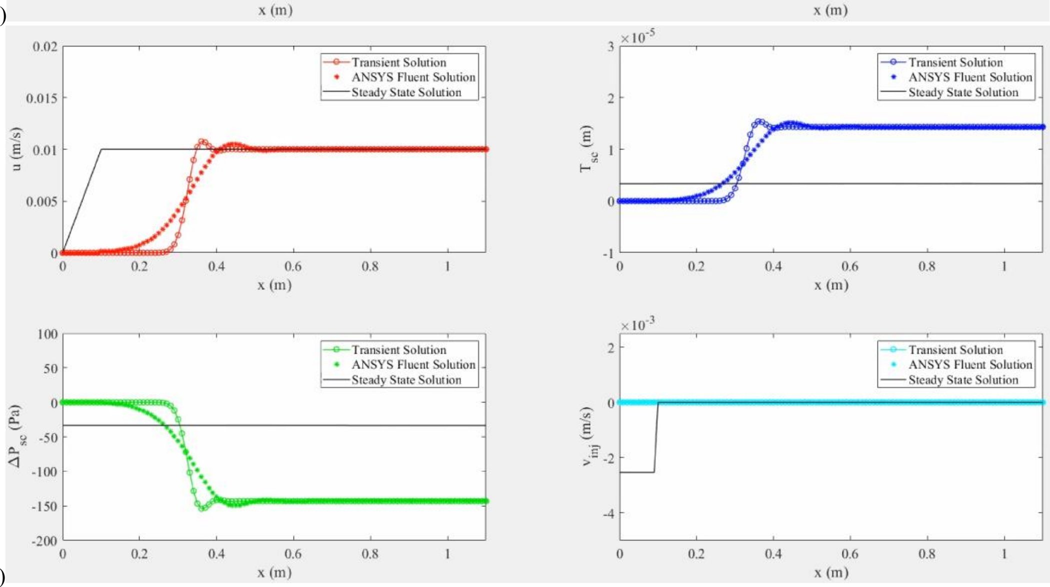

B)

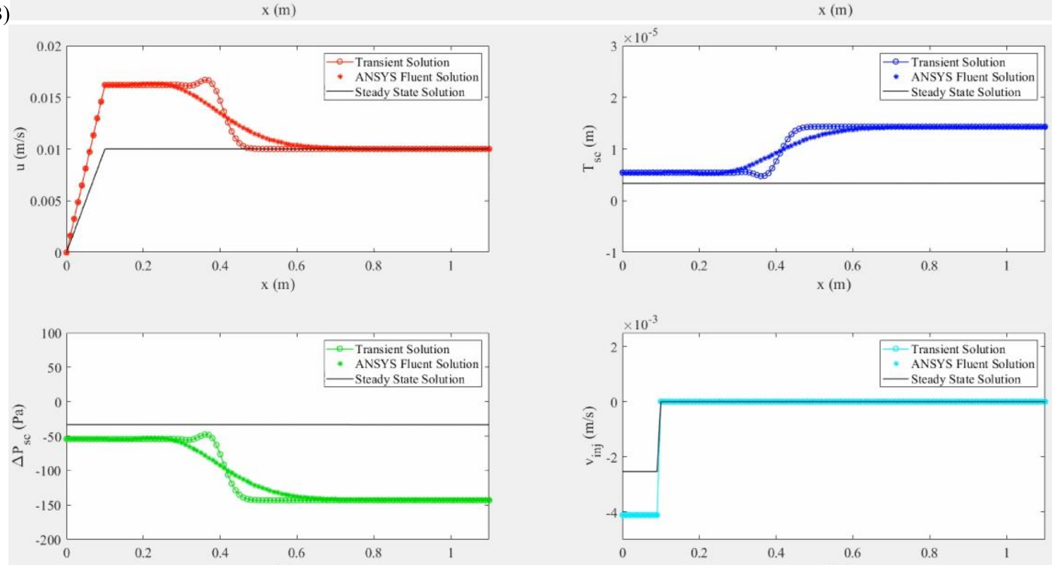

C)

Fig. 14. Comparison of the transient screen compliance solver and ANSYS Fluent results at A) $t = 0.015\ s$, B) $t = 0.045\ s$, and C) $t = 0.075\ s$.

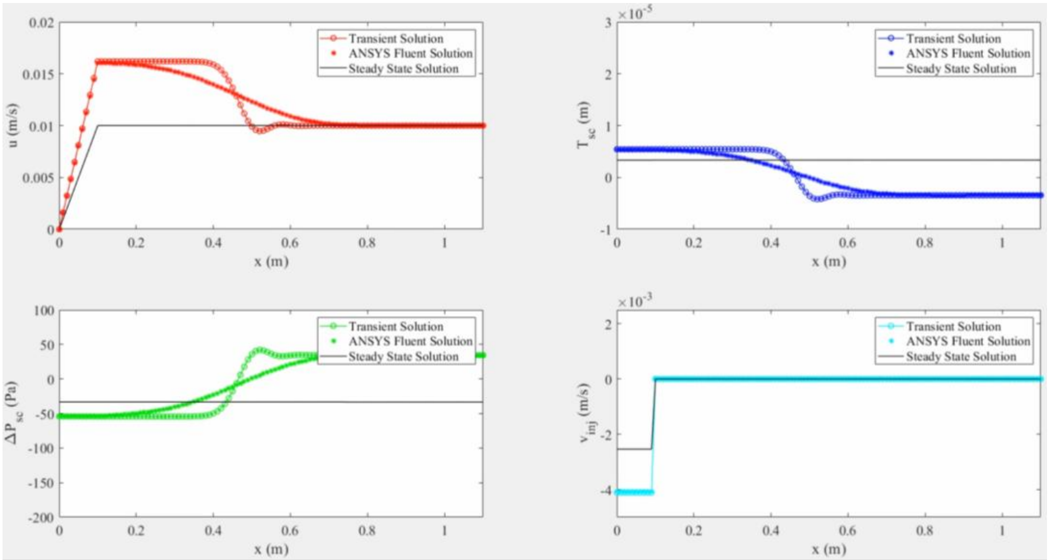

A)

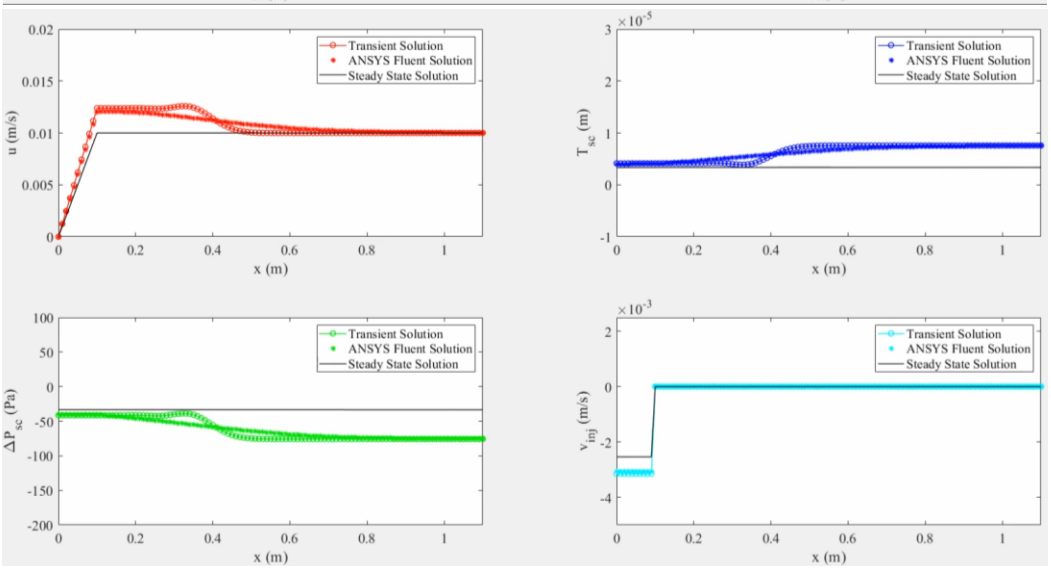

B)

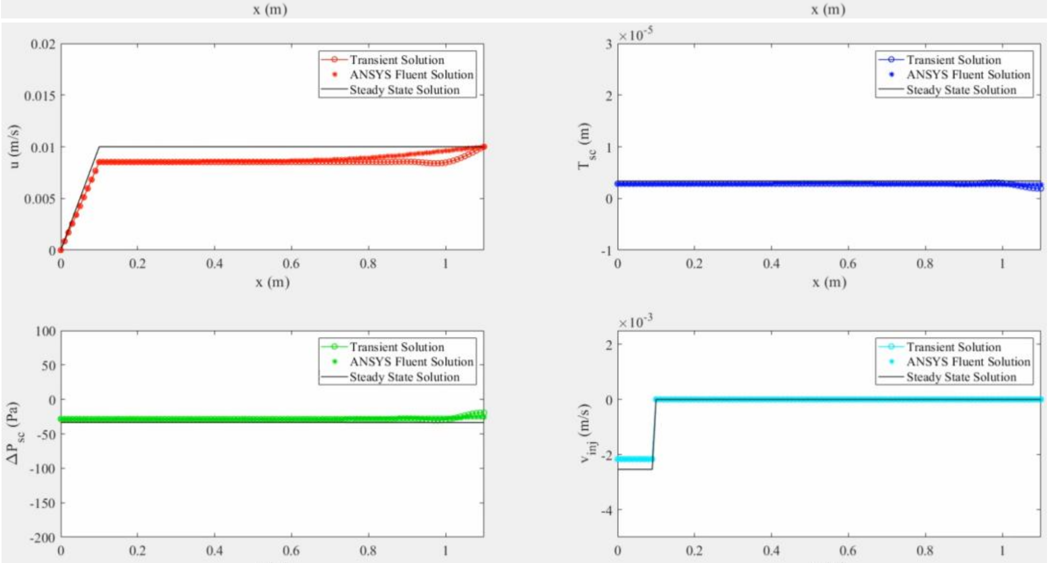

C)

Fig. 15. Comparison of the transient screen compliance solver and ANSYS Fluent results at A) $t = 0.15\ s$, B) $t = 0.30\ s$, and C) $t = 0.45\ s$.

Table 3. Inputs for transient screen compliance solver and ANSYS Fluent solver comparison. Note that for the ANSYS Fluent solver, transient screen compliance solver fluid properties are used in the submerged boundary condition UDF. Furthermore, the ANSYS Fluent submerged boundary condition UDF neglects viscous pressure drop effects along the channel since these effects are considered negligible for such a short submerged portion of the channel.

Input	Transient Screen Compliance Solver	ANSYS Fluent Solver
Fluid	Liquid Nitrogen	Liquid Nitrogen
Density, ρ (kg/m^3)	807.7	806.1
Viscosity, μ $(Pa \cdot s)$	1.63e-4	1.61e-4
Screen Type	325x2300	325x2300
Screen Compliance Constant, K_{SC} (Pa/m)	1e7	1e7
Channel Height, H (m)	0.0254	0.0254
Channel Width, w_{sc} (m)	0.0254	0.0254
Exposed Channel Length, $L_{exposed}$ (m)	1	1
Submerged Channel Length, $L_{submerged}$ (m)	0.1	0.1
Demand Velocity Profile to Steady State	Step Change	Step Change
Steady State Demand Velocity, u_{demand} (m/s)	0.01	0.01
Gravity, g (m/s^2)	0	0
Submerged Boundary Condition	Method 2	Method 2
Number of Exposed Grid Points, $N_{x,exposed}$	101	N/A
Number of Submerged Grid Points, $N_{x,submerged}$	11	N/A
Time Step, Δt (s)	0.0005	0.0005
Viscous Model	See discussion	Laminar
Number of Cells in x-direction (ANSYS only)	N/A	100
Number of Cells in y-direction (ANSYS only)	N/A	4
Pressure Under-Relaxation Factor (ANSYS only)	N/A	0.0002
All Other Under-Relaxation Factors (ANSYS only)	N/A	Kept as ANSYS default
Pressure Velocity Couple (ANSYS only)	N/A	SIMPLE
Spatial Gradient Discretization (ANSYS only)	N/A	Green-Gauss Node Based
Spatial Pressure Discretization (ANSYS only)	N/A	PRESTO!
Spatial Momentum Discretization (ANSYS only)	N/A	Third-Order MUSCL
Transient Formulation (ANSYS only)	N/A	First Order Implicit

V. GENERAL DISCUSSION

One of the purposes of this section will be to highlight a few approximations taken as part of this analysis. The first approximation involves the application of the submerged section solver at the submerged end boundary condition. The second approximation involves assuming that K_{SC} does not change as a function of x. The third approximation involves the simplified viscous term used as part of this 1D model. The implications of these highlighted approximations will be discussed, and potential future work will be addressed. After highlighting these approximations, a recommended safety factor for transient screen compliance analysis will be presented and a few concluding remarks will be made.

The first highlighted approximation involving the application of the submerged section solver (i.e. Method 1 or Method 2) is taken in order to couple the 1D transient screen compliance solver used on the exposed section of the channel with the steady solver used on the submerged end of the channel. As discussed, the coupling involves extrapolating a velocity at the submerged end boundary of the exposed section of the channel and inputting the value into the steady submerged solver for each timestep. This coupling methodology introduces a quasi-transient submerged section of the channel. In other words, a steady state solver is updated for the submerged end of the channel at each time step. The main implicit assumption taken with this coupling methodology is that the injection velocity is fully developed for each time step. A theoretical case could be made that the effects of this approximation are negligible. Since the demand mass flow on the submerged portion of the channel is satisfied by an injection velocity and not screen deflection, it is expected that the submerged section of the channel would have incompressible flow characteristics (i.e. the characteristic wave propagation speed would be very large). This would allow for the submerged boundary to instantaneously communicate with the entire submerged section of the channel; however, it still does not directly address the assumption that the submerged injection velocity is fully developed at each timestep. It would need to be determined empirically if the effects of this approximation are negligible or if a separate transient 2D submerged section solver needs to be developed.

A more consequential approximation may involve the second highlighted approximation that K_{SC} is not a function of x. The approximation implicitly enforces T_{SC} being an effective deflection thickness and not an actual deflection thickness. In other words, K_{SC} is simply used to couple mass and momentum by providing a relationship between ΔP_{SC} and T_{SC} via the equation of state. If T_{SC} was an actual deflection thickness, then a boundary condition of $T_{SC} = 0$ would need to be enforced at the fixed demand end of the channel. Therefore, to capture actual screen deflection, K_{SC} would need to vary with respect to x (i.e. it is expected that the screen would not deflect as much near the fixed boundaries and deflect more towards the middle of the channel). The consequence of this approximation could be a $\Delta P_{SC}'$ increase at the demand end of the channel since the actual screen would not be able to deflect as much at that location. Another consequence of K_{SC} not being a function of x is that the characteristic speed for the exposed section of the channel does not vary as a function of x. If K_{SC} is varied as a function of x, the characteristic speed would vary along the exposed section of the channel. If it is determined that this approximation is not negligible, the equation of state would need to be modified to make K_{SC} a function of x. This would most likely require additional testing and analysis.

The final highlighted approximation is a rather simple point to make and involves the modified viscous term that is being used as a part of this study. As discussed, the current form of the screen compliance model is 1D and needs to implement a modified viscous term to properly account for steady state pressure drop. The modified viscous term used was taken from Hartwig et al. 2014 [6] which assumes a steady state velocity profile in the channel. For highly turbulent transient flows, this approximation may not be very accurate. However, as discussed in Hartwig et al. 2014, the viscous effects during LAD channel operation are considered second order in a microgravity environment. Therefore, the additional analysis required to properly analyze transient 3D turbulent flow during LAD screen compliance may not be necessary in this application.

It is important that this model be validated with empirical data. The fact that this transient model shows significantly higher $\Delta P_{SC_{max}}'$ values than the steady state model indicates that if transient screen compliance is not properly accounted for during LAD operation, a large amount of vapor could be ingested into the channel. An example of the difference between $\Delta P_{SC_{max}}'$ values at steady state and during a transient can be seen in Fig. 14 and Fig. 15 where transient values are approximately three times higher than steady state values. Part of the empirical work should determine which assumptions and approximations are appropriate and which ones introduce unacceptable amounts of error. The result of the model validation will allow for smaller transient safety factors to be used and increased confidence in transient LAD channel design. Jaekle 1997 [1] recommends a relatively large safety factor of two or three to be used on the bubble point value in conjunction with this transient screen compliance analysis.

VI. CONCLUSION

This study developed and verified a transient LAD outflow solver using a new model that has been modified from the original screen compliance model from Jaekle 1997 [1] and the equation of state developed by Camarotti et al. 2019 [2]. The viscous term in the 1D transient screen compliance model has been modified to ensure that a viscous pressure drop along the channel can exist at steady state that matches historically developed steady state models. Along with modifying the viscous term, a derivation has been provided for the 1D transient screen compliance model that had not been previously developed. The characteristic speed of the governing equations has been found and used to establish the transient screen compliance solver stability criteria for the Two-Step Lax-Wendroff method of Rubin and Burstein used in this solver. The solver was verified using a mesh refinement analysis, Generalized RH Condition analysis, and a comparison with ANSYS Fluent.

It has been concluded that the understanding of LAD transient screen compliance is crucial for successful LAD operation. As shown in this study, the transient maximum pressure difference across the screen can greatly exceed the steady state maximum pressure difference across the screen in many cases. For example, the transient pressure difference across the screen for the sample case shown in Fig. 14 and Fig. 15 is approximately three times higher than the steady state pressure difference across the screen. As a result, it is important that this model be validated with empirical data to determine if the assumptions and approximations taken in this model are warranted or if additional analysis is needed. Currently, Jaekle 1997 [1] recommends a safety factor of two or three to be used on the bubble point value in conjunction with this transient screen compliance analysis due to the approximations taken as part of this model. Validating the transient screen compliance model with empirical data will allow for smaller transient safety factors to be used and an increased confidence in transient LAD channel design.

VII. REFERENCES

[1] D. E. Jaekle, Jr., "AIAA-97-2811 Propellant Management Device Conceptual Design and Analysis: Galleries," in *33rd*

AIAA/ASME/SAE/ASEE Joint Propulsion Conference & Exhibit, Seattle, WA, 1997.

[2] C. Camarotti, O. Deng, S. Darr, J. Hartwig and J. N. Chung, "Screen Compliance Experiments for Application of Liquid Acquisition Device in Space," *Microgravity Science and Technology,* vol. 31, pp. 109-122, 2019.

[3] H. Paynter, "Final Report Acquisition/Expulsion System for Earth Obital Propulsion System," Martin Marietta Corporation, Denver, Colorodo, 1973.

[4] C. Camarotti, J. Hartwig, D. Yaegers, S. Vasireddy and J. Chung, "The Effect of Liquid Withdrawal Rate on Screen Channel Liquid Acquisition Device Screen Compliance," *Microgravity Science and Technology,* vol. 34, no. 86, 2022.

[5] S. Vasireddy, C. Camarotti, J. Hartwig and J. Chung, "Liquid Acquisition Device Screen Compliance Experiments with Rectangular Geometry for Microgravity Applications," *Microgravity Science and Technology,* vol. 34, no. 2, 2022.

[6] J. W. Hartwig, S. R. Darr, J. B. McQuillen, E. Rame and D. J. Chato, "A steady state pressure drop model for screen channel liquid acquisition devices," *Cryogenics,* vol. 64, pp. 260-271, 2014.

[7] S. Darr, C. Camarotti, J. Hartwig and J. Chung, "Hydrodynamic model of screen channel liquid acquisition devices for in-space cryogenic propellant management," *Physics of Fluids,* vol. 29, 2017.

[8] P. K. Kundu, I. M. Cohen and D. R. Dowling, Fluid Mechanics, 6th ed., Elsevier, 2016.

[9] J. Hartwig and S. Darr, "Analytical model for steady flow through a finite channel with one porous wall with arbitrary suction or injection," *Physics of Fluids,* vol. 26, 2014.

[10] D. E. Jaekle, Jr., "Propellant Management Device Conceptual Design and Analysis: Vanes," in *AIAA/SAE/ASME/ASEE 27th Joint Propulsion Conference*, Sacramento, CA, 1991.

[11] J. Armour and J. Cannon, "Fluid flow through woven screens," *AIChE,* vol. 14, no. 3, pp. 415-420, 1968.

[12] E. L. Rubin and S. Z. Burstein, "Difference Methods for the Inviscid and Viscous Equations of a Compressible Gas," *Journal of Computational Physics,* pp. 178-196, 1967.